Low Complexity Methods for Joint Detection and Synchronization of TDMA Bursts

Haotian Zhai and Bernd-Peter Paris
Department of Electrical and Computer Engineering
George Mason University
Fairfax, VA 22030
{hzhai,pparis}@gmu.edu

Abstract—This paper proposes a data-aided joint detection and carrier synchronization algorithm for TDMA bursts. A sequential detection algorithm based on the generalized likelihood ratio test (GLRT) is used to detect the embedded preamble signal in received data stream. Carrier synchronzation happens during sequential detection to provide carrier estimates for GLRT and after detection to compute accurate estimates for coherent demodulation. Thus, we propose a family of estimators with low-complexity and high-accuracy to accommodate for the two cases. At the end, the complete joint detection and estimation algorithm is validated through simulation and SDR at a very high sample rate.

I. Introduction

In digital communication systems, information is commonly transmitted in time-multiplexed bursts. Examples include time-slotted random access systems. Each active user transmits information to the receiver in the same frequency band and in non-overlapping time intervals [1]. A fundamental prerequisite for successful coherent demodulation is that the receiver can detect the beginning of the data stream and estimate accurately the phase and frequency offset of the carrier. It is worth emphasizing that time and carrier synchronization are coupled problems, especially at low SNRs: coherent methods for detecting the signal require accurate frequency and phase estimates while data-aided frequency and phase estimation requires that the location of the training sequence is available. Thus, joint signal detection and carrier synchronization algorithms play a vital role in any communication system.

Clearly, the signal acquisition problem has been considered widely. In the late 90's, Morelli and Mengali [2] presented a tutorial review of the carrier synchronization field comparing such characteristics as estimation accuracy, range, and computational complexity of available techniques. The work by [3]–[5] is most related to results in this paper. For signal detection, particularly, sequential detection process, most of the sequential detector is built based on hypothesis testing [6]–[8]. Moreover, the lack of information happens commonly when build likelihood ratio test (LRT). For example, the LRT in [7] is built based on the distribution of data stream, which is unknown. The LRT is then replaced by generalized likelihood ratio test.

In this paper, we propose a joint detection and estimation algorithm for the signal acquisition process and implement it on software-defined radio (SDR). In particular, the detection algorithm operates sequentially for every incoming sample and is built based on the estimates from the carrier synchronization.
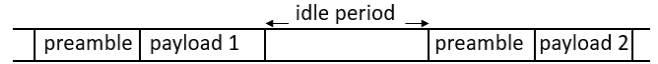

Fig. 1. Structure of signal stream at the receiver

Thus, a family of low-complexity and high-accuracy estimators is proposed for implementing in sequential detection and coherent demodulation on SDR at very high sample rate.

II. Signal Model

In an uplink multiuser system, the transmitted signal frame from each user is seperated by an unkown length of idle period and assumed to include a reference signal that is known to the receiver. Often such a reference sequence is prepended to the payload and is referred to as a preamble. The structure of signal stream at the receiver is shown in Figure 1. The problem addressed in this paper is to accurately estimate the start time of the preamble and to estimate carrier phase and frequency offset from the preamble. Hence, the payload portion of the frame is not further considered.

We now give the signal model for this paper. The received RF signal is first modulated at base band. In [2] and [6], the authors obtain a simplifed signal model from the matched filter outputs by assuming the symbol time is perfectly known. However, in practice, this is unreliable especially at low SNR. To accommodate this issue, we analyze the discrete signal model directly after down-conversion and sampling, which yields received samples r_n

$$r_n = s_{n-\bar{p}} A e^{j\phi} e^{j2\pi\delta n} + w_n, \tag{1}$$

where s_n denotes the sampled reference sequence (the preamble), which has the form

$$s_n = \sum_{i=0}^{L_0-1} c_i g(nT_s - iT) \quad \text{for } n = 0, \dots, N-1, \tag{2}$$

In (1), $\bar{p}$ denotes the start position of the received preamble. Note, because of the uncertainty of sampling, often the sampler may not sample exactly at the start time of the preamble, which causes the integer delay $\bar{p}$ with a fractional delay in the range of $[-\frac{T_s}{2}, \frac{T_s}{2})$, where T_s is the sample period as in (2). In this paper, the sampling rate is assumed to be high enough relative
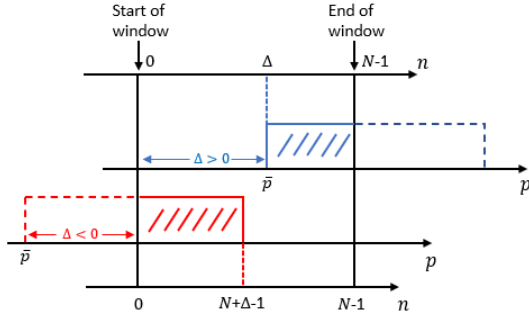
Fig. 2. Two cases of detection when a portion of the preamble is in window

to the symbol rate, so that the influence of fractional delay can be ignored. A, ϕ, δ are the amplitude, carrier phase and normalized frequency offset with respect to sample period T_s that we want to estimate. w_n is complex AWGN. Moreover, E_s/N_0 denotes the ratio of signal energy to noise power spectral density (SNR). To make analysis easier, we assume a constant and normalized envelope of the samples in the preamble, i.e., $A^2|s_n|^2 \approx A^2 = E_s/M$ for $n = [0, N-1]$, where M is the rate of oversampling in each symbol of the preamble.

In (2), T denotes the symbol period and $g(t)$ provides pulse shaping. $\{c_i\}_{i=0}^{L_0-1}$ is the symbol sequence known at transmitter and receiver, where L_0 denotes the number of symbols. We define $N = ML_0$ to be the number of samples in the preamble. Note, compared with the signal model in [2] and [6], by using an oversampled signal, we can mitigate the coherent loss that occurs when the signal with frequency offset is passed through the matched filter. This allows our system to tolerate larger frequency offsets.

III. DETECTION AND TIME SYNCHRONIZATION

We start by looking at the two hypotheses for the sequential detection task: Let H_0 be the null hypothesis that the received signal is the channel noise or only contains a portion of the preamble against the alternative H_1 that it contains the entire preamble. Define Δ to be the distance between the current start position of the window of N received samples and the start position of the preamble $\bar{p}$. Figure 2 illustrates two cases when a portion of the preamble is in the window with global delay index p and local sample index n. Thus, for $n = 0, 1, \ldots, N-1$, the two hypotheses are given by the window of samples r_n

$$H_0: r_n = \begin{cases} s_{n-\Delta}\xi e^{j2\pi\delta(n-\Delta)} + w_n & \max(0,\Delta) \leq n < \min(N, N+\Delta) \\ w_n & \text{otherwise,} \end{cases}$$
$$H_1: r_n = s_n\xi e^{j2\pi\delta n} + w_n.$$
$$(3)$$

where $\xi = Ae^{j\phi}$ denotes the phasor in (1). Furthermore, $\Delta \neq 0$ is the premise under hypothesis H_0 while $\Delta = 0$ under H_1.

In this paper, we focus on discussing when a portion of the preamble occurs in the window and $\Delta \in (0, N-1]$, which refers to the top case in figure 2. The bottom case when $\Delta \in [-N+1, 0)$ is omitted discussing because it is symmetric to the top case. Based on (3), we build conditional likelihood ratio test (CLRT)

between H_0 and H_1 by giving the distance Δ, the phasor ξ and the frequency offset δ at position $\bar{p}$. The likelihood ratio is given by

$$\Lambda(R|\Delta, \xi, \delta) = \frac{f_{R|H_1, \xi, \delta}(r|H_1, \xi, \delta)}{f_{R|H_0, \Delta, \xi, \delta}(r|H_1, \Delta, \xi, \delta)}$$

$$= \frac{\prod_{n=0}^{N-1} \frac{1}{\sqrt{\pi N_0}} e^{-\frac{|r_n - s_n\xi e^{j2\pi\delta n}|^2}{N_0}}}{\frac{1}{(\pi N_0)^{N/2}} \prod_{n=\Delta}^{N-1} e^{-\frac{|r_n - s_{n-\Delta}\xi e^{j2\pi\delta(n-\Delta)}|^2}{N_0}} \prod_{n=0}^{\Delta-1} e^{-\frac{|r_n|^2}{N_0}}}$$

$$\underset{H_0}{\overset{H_1}{\gtrless}} \eta.$$
$$(4)$$

Cancelling the common parts and taking the logarithm, (4) is reduced to

$$\Re\left\{ \sum_{n=0}^{N-1} r_n s_n^* \xi^* e^{-j2\pi\delta n} - \sum_{n=\Delta}^{N-1} r_n s_{n-\Delta}^* \xi^* e^{-j2\pi\delta(n-\Delta)} \right\} \underset{H_0}{\overset{H_1}{\gtrless}}$$
$$\frac{N_0}{2} \ln \eta + \frac{A^2}{2} \sum_{n=N-\Delta}^{N-1} |s_n|^2.$$
$$(5)$$

On the left hand side, the two summations are the matched filters for hypothesis H_1 and H_0, respectively. It can be derived the principal value of the left hand side of (5) reduces to the difference between the energy of the preamble and a "partial" autocorrelation function (ACF) of the preamble at lag Δ under two hypotheses. Moreover, we notice the second summation on the left hand side is not computable due to the unknown information of Δ while the first summation is. On the other hand, the first summation reflects the energy of the preamble under H_1 and the "partial" ACF of the preamble at lag Δ under H_0. Note, the effect of the "partial" ACF can be mitigated by using the preamble with a good autocorrelation property.

Thus, a practical sequential detector is built just based on the cross-correlation between the received signal and the preamble corrected by the frequency and phasor estimates with some proper scaling. Specifically,

$$\rho(p) = \frac{\Re\{\langle \boldsymbol{r}_p, \hat{\boldsymbol{s}}_p \rangle\}}{||\boldsymbol{r}_p|| \cdot ||\hat{\boldsymbol{s}}_p||} \underset{H_0}{\overset{H_1}{\gtrless}} \gamma$$
$$(6)$$

where $\boldsymbol{r}_p = [r_p, r_{p+1}, \ldots, r_{p+N-1}]$ denotes the window of received signal sequence at position p. $\hat{\boldsymbol{s}}_p$ denotes the carrier-corrected preamble, where each element is $\hat{s}_n = s_n\hat{\xi}_p e^{j2\pi\hat{\delta}_p n}$ for $n = 0, 1, \ldots, N-1$, and $\hat{\xi}_p$, $\hat{\delta}_p$ are the carrier estimates at position p. $||\cdot||$ is the Euclidean norm of the signal sequence, and γ is the normalized detection threshold which lies in the range of $[0, 1]$. From (6), we see a realistic generalized likelihood ratio test (GLRT) replaces the CLRT by first doing the carrier synchronization of signal in window at each position and then plugging the estimates in the LRT. It should be emphasized that our detector requires to work at high sample rate; While (6) is straightforward and of complexity $O(N)$, the

complexity of estimating $\hat{\xi}, \hat{\delta}$ is critical for practical implementation. A pair of low-complexity frequency and phasor estimates will be given in the next section.

IV. FREQUENCY AND PHASE ESTIMATION

In this section, estimation is performed using a window of N samples, $0 \le n < N$, starting at the position $\bar{p}$ of the preamble. For estimating the frequency offset δ and phasor $\xi = Ae^{j\phi}$, the maximum likelihood estimation (MLE) of the parameters in (1) is given by

$$\hat{\delta}, \hat{\xi} = \min_{\delta, \xi = Ae^{j\phi}} \sum_{n=0}^{N-1} |r_n - s_n \xi e^{j2\pi\delta n}|^2. \tag{7}$$

A closed form for $\hat{\xi}$ is readily derived by taking the Wirtinger derivative with ξ and setting it equal to zero,

$$\hat{\xi} = \frac{\sum_{n=0}^{N-1} r_n s_n^* e^{-j2\pi\hat{\delta}n}}{\sum_{n=0}^{N-1} |s_n|^2}, \tag{8}$$

so that $\hat{\xi}$ relies on the frequency estimate $\hat{\delta}$, and $\hat{\phi} = \arg\{\hat{\xi}\}$.

A necessary condition for the frequency offset estimate $\hat{\delta}$ is obtained similarly by taking the derivative of (7) with respect to δ and setting it equal to zero. Skipping all intermediate derivation steps for brevity's sake, it yields

$$J(\hat{\delta}) = \Im\left\{ \sum_{k=1}^{N-1} \sum_{m=k}^{N-1} k r_{m-k} r_m^* s_{m-k}^* s_m e^{j2\pi\hat{\delta}k} \right\} = 0. \tag{9}$$

There are a number of local minima of (7) also satisfying the necessary condition for $\hat{\delta}$ of (9) in addition to the absolute minimum (the exact solution of MLE). In [5] and [4], the "false minima" are avoided by appropriately restricting the operating range of the estimator. Specifically, instead of calculating the sample autocorrelation functions for all lags $k \in [1, N-1]$, they truncate (9) by only considering the lag autocorrelation functions for $k \in [1, \varepsilon]$, where $\varepsilon \ll N-1$. This is to avoid including the inner summations in (9) with few terms and correspondingly high variance.

Moreover, the estimator $\hat{\delta}$ in (9) has no closed-form solution. In [5], the necessary condition is approximated by replacing the exponential with its Taylor series expansion. In [4], an approximate solution is obtained via Euler's identity for large N. Both L&R [5] and Fitz [4] estimators have computational complexity $O(N^2)$ reflecting the double summation. In [3], the Kay estimator reduces the complexity from $O(N^2)$ to $O(N)$ by only computing (9) at lag $k = 1$. However, it suffers from poor accuracy at low SNRs.

In this paper, we propose a family of alternative solutions to (9). A coarse solution with $O(N)$ complexity is used for operating at high sample rate during the sequential detection. It prioritizes low complexity at the expense of some loss of accuracy. A second more accurate solution is used to improve the estimation accuracy at moderate complexity to enable coherent demodulation once the preamble has been detected.

A. Coarse Solution: Single-Lag Estimator with Length-v Partial Correlating

The first estimator is rooted in the insight that at high SNR, every lag k in (9) can be used to approximate the frequency estimate δ. By setting $r_m \approx s_m \xi e^{j2\pi\delta m}$, (9) is expanded to

$$\Im\left\{ A^2 \sum_{k=1}^{N-1} \sum_{m=k}^{N-1} k |s_{m-k}|^2 |s_m|^2 e^{j2\pi(\hat{\delta}-\delta)k} \right\} = 0. \tag{10}$$

Note, the inner summation in (10) is purely real for every lag k if $\hat{\delta} = \delta$. This suggests that an unbiased estimate of δ can be obtained by using only a single lag k. The approach yields a closed-form solution for $\hat{\delta}$, which is given by

$$\hat{\delta}_{SL}(k) = -\frac{\arg\left\{ \sum_{m=k}^{N-1} r_{m-k} r_m^* s_{m-k}^* s_m \right\}}{2\pi k}, \tag{11}$$

However, the above single-lag (SL) estimator has insufficient accuracy at low SNRs as we will show below. To extend range of operation to low SNR, an alternative SL estimator including partial coherent integrator prior to estimation is given by

$$\hat{\delta}_{SL}^{(v)}(k_v) = -\frac{\arg\left\{ \sum_{l=k_v}^{N/v-1} F_l^{*(v)} F_{l-k_v}^{(v)} \right\}}{2\pi k_v v}, \tag{12}$$

where F denotes the result of coherent integration of length-v blocks

$$F_l^{(v)} = \sum_{n=lv}^{(l+1)v-1} r_n s_n^*, \quad \text{for } l = 0, 1, \ldots, N/v-1. \tag{13}$$

Normally, v is set to be a factor of N to include all the sample instants with maximum $v = N/2$. In (12), $k_v = \lfloor k/v \rfloor$ denotes the distance between blocks that we want to estimate carriers from. $\lfloor \cdot \rfloor$ is the floor operator. It can be seen (11) is the special case of (12) when $v = 1$, meaning no partial integrator is used.

1) Performance of single-lag estimator: For evaluating the performance of the SL estimator, we first look at the probability density function (pdf) of the coherent integration $F_l^{*(v)}$ in (12). By setting $r_n = s_n \xi e^{j2\pi\delta n} + w_n$ into (13), $F_l^{*(v)}$ yields a complex Gaussian random variable (r.v.) with pdf

$$F_l^{*(v)} \sim CN\left(\xi^* \sum_{n=lv}^{(l+1)v-1} e^{-j2\pi\delta n}, \frac{N_0}{2} v \right), \tag{14}$$

where $A^2 |s_n|^2 \approx A^2 = E_s/M$ is hold by assuming a constant and normalized envelope of the preamble given in Section II. Note, $F_l^{*(v)}$ and $F_{l-k_v}^{(v)}$ are uncorrelated. Based on (14), the product $C_F(v, l) = F_l^* F_{l-k_v}$ has a mixed distribution of a complex Gaussian and a second kind Bessel function from the products of noise terms. The mean μ_{C_F} and variance $\sigma_{C_F}^2$ of $C_F(v, l)$ are given by, respectively

$$\mu_{C_F} = \frac{E_s}{M} \sum_{n=lv}^{(l+1)v-1} e^{-j2\pi\delta n} \left(\sum_{m=(l-k_v+1)v}^{(l-k_v+1)v-1} e^{j2\pi\delta m} \right)$$

$$= E_s/M \cdot e^{-j2\pi\delta k_v v} \mathcal{D}^2(v,\delta), \qquad (15)$$

$$\sigma_{C_F}^2 = \underbrace{N_0^2 v^2/4}_{\text{from Bessel}} + \underbrace{N_0 E_s v/M \cdot \mathcal{D}^2(v,\delta)}_{\text{from Complex Gaussian}},$$

where $\mathcal{D}(v,\delta) \triangleq \frac{\sin(\pi\delta v)}{\sin(\pi\delta)}$ is the Dirichlet function of δ, which approaches the maximum value v at $\delta = 0$ and first two zeros at $\delta = \pm 1/v$. Note, both μ_{C_F}, $\sigma_{C_F}^2$ are independent of the partial integration block. Thus, the mean and variance of $\sum C_F$ in the argument operator of (12) satisfy $\mu_{\sum C_F} = \sum \mu_{C_F}$ and $\sigma_{\sum C_F}^2 = \sum \sigma_{C_F}^2$.

Recall from (12), the distribution of SL estimator depends on $\arg\{\cdot\}$. It can be shown that the full pdf of $\arg\{\zeta\}$, where ζ is complex Gaussian distributed, is well approximated for moderate SNR, as Gaussian. Specifically,

$$\arg\{\zeta\} \sim \mathcal{N}\left(\angle\mu_\zeta, \sigma_\zeta^2/|\mu_\zeta|^2\right). \qquad (16)$$

The derivation of (16) is omitted due to space constraint. Based on (16), the performance evaluation of the SL estimator can be obtained by looking at the variance in (16), or equivalently, the "output" SNR, which equals to the absolute square of mean to variance of $\sum C_F$ in the argument operator of (12), i.e.,

$$\text{SNR}_{out}^{(v,\delta)} = \frac{|\mu_{\sum C_F}|^2}{\sigma_{\sum C_F}^2} = \frac{(N/v - k_v) \cdot \mathcal{D}^4(v,\delta)}{v^2/\text{SNR}_{in} + 2v \cdot \mathcal{D}^2(v,\delta)} \cdot \text{SNR}_{in}. \qquad (17)$$

where $\text{SNR}_{in} = 2E_s/(MN_0)$. From (17), we see the "output" SNR is degraded by the variance of second kind Bessel r.v. at low input SNRs. By assuming a small frequency offset, e.g., $|\delta|v \ll 1$, the relative processing gain with and without partial correlating is given by

$$\frac{\text{SNR}_{out}^{(v)}}{\text{SNR}_{out}^{(1)}} \approx \frac{v + 2v \cdot \text{SNR}_{in}}{1 + 2v \cdot \text{SNR}_{in}}. \qquad (18)$$

Some observations can be obtained from (18). First, we see the maximum relative processing gain approaches v as SNR_{in} approaches 0. Moreover, when the input SNR is fixed and small, the relative processing gain is increased as v becomes larger. On the other hand, at high input SNRs, the effect of Dirichlet function in (17) becomes more important than the relative processing gain. Thus, the SNR_{out} approaches the maximum with $v = 1$.

Based on (11), (15) and (16), the distribution of $\hat{\delta}_{SL}^{(v)}(k_v)$ at moderate SNRs is finally given by

$$\hat{\delta}_{SL}^{(v)}(k_v) \sim \mathcal{N}\left(\delta, \frac{(Mv + 4\mathcal{D}^2(v,\delta) \cdot E_s/N_0) \cdot Mv}{16\pi^2 k^2 (N/v - k_v)(E_s/N_0)^2 \mathcal{D}^4(v,\delta)}\right). \qquad (19)$$

Thus, $\hat{\delta}_{SL}^{(v)}(k_v)$ is unbiased. A lower bound for the variance of single-lag estimator at high SNRs is obtained as the variance

	Complex products	Complex additions
$\hat{\delta}_{SL}^{(1)}(k)$	$N/3 + 1$	$N/3$
$\hat{\delta}_{SL}^{(v)}(k_v)$	$(2 + 1/v)N/3$	$(2 - 1/v)N/3 - 1$

of (19) when $v = 1$. Moreover, we can see the variance also depends on the value of k_v. The best choice for k_v is to choose $k_v = \lfloor \frac{2N}{3v} \rfloor$ to minimize the variance.

2) Estimation range: The SL estimator may suffer an effect of "aliasing" akin to $2\pi|\delta|k_v v > \pi$. Thus, a safe estimation range for the estimator with optimal $k_v = \lfloor \frac{2N}{3v} \rfloor$ to avoid modulo-2π ambiguity is δ within $\pm 3/(4MN)$. Compared with the same autocorrelation-based estimator, e.g., the L&R [5] and Fitz [4], single-lag estimator has 3/8 estimation range of L&R and 3/4 estimation range of Fitz.

3) Computational complexity: We have discussed the accuracy of single-lag estimator. It is also necessary to address the complexity since the SL estimator is used in high sample-rate case. The computational complexity of single-lag estimator can be readily assessed from (12), (13) and (11).

Specifically, we compare with the complexity of SL estimators in sequential detection with and without partial correlating. Note, without partial correlating, from (11), $s_{m-k}^* s_m$ can be precomputed and stored like "filter coefficients"; Moreover, due to the characteristic of the sequential detection process, the products of received samples, $r_{m-k} r_m^*$, can be stored in a shift register so that only one new product needs to be computed per sample period.

The exact computational complexity of two single-lag estimators are given in Table I with optimal $k_v \approx 2N/(3v)$. We see $\hat{\delta}_{SL}^{(1)}(k)$ has approximate 2 times fewer complex products and additions compared with $\hat{\delta}_{SL}^{(v>1)}(k_v)$ in sequential detection. Furthermore, note the complexity of Kay estimator in [2] is given approximately $3N/4$ complex products and additions, which is slightly bigger than $\hat{\delta}_{SL}^{(1)}(k)$.

B. Fine Solution: Newton-Method based Estimator

The SL estimator emphasizes low-complexity property and is intended to provide merely sufficient good carrier synchronization to enable coherent detection. Once the signal has been acquired, the SL estimator can be improved by investing additional computations. Since detection events are rare, the computational complexity is of little concern.

The principle of Newton-Method based estimator is to use the single-lag estimator as the starting point for a Newton-type iteration aimed at finding a better solution to the necessary condition (9). In principle, multiple iterations are possible to produce successively better approximations to the root of $J'(\cdot)$ in (9). Specifically, the iterations are given by

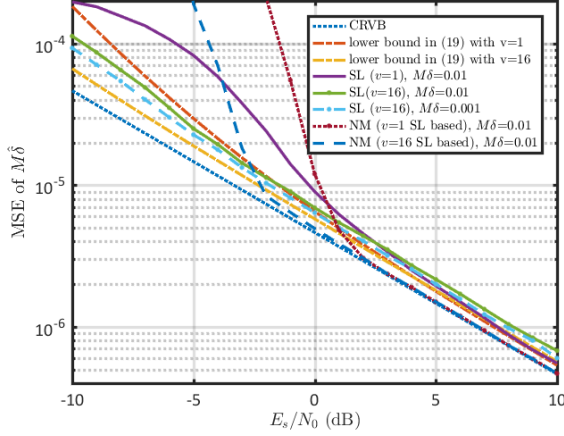$$\hat{\delta}_{NM}^{(i+1)} = \hat{\delta}_{NM}^{(i)} - \frac{J(\hat{\delta}_{NM}^{(i)})}{J'(\hat{\delta}_{NM}^{(i)})} \qquad (20)$$

Fig. 3. Accuracy of the NM estimator and single-lag estimator ($L_0 = 32$)

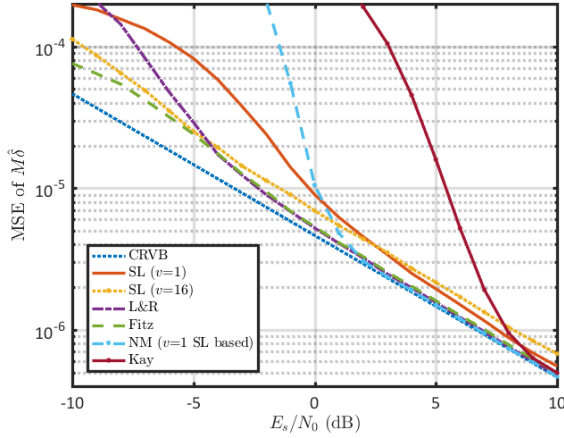Fig. 5. Receiver operating characteristics (ROC) of the sequential detector

Fig. 4. Accuracy of SL, NM and traditional estimators ($L_0 = 32$, $M\delta = 0.01$)

where $\hat{\delta}_{NM}^{(0)} = \hat{\delta}_{SL}^{(v)}(k_v)$ is the starting point of iteration and $J'(\cdot)$ denotes the derivative of J with respect to $\hat{\delta}$. Our simulations indicate that only a single iteration is usually sufficient to achieve very good accuracy.

We can conclude the importance of accuracy of the SL estimator at low SNRs: with a merely sufficient good accuracy, the SL estimator not only increases the probability of detection by better fitting the preamble and received signal as in sequential detector (6), but it provides a reasonable starting point for getting the more accurate NM estimator. In simluations, we will also show the case when the NM estimator has a worse accuracy than the SL estimator if the latter does not provide enough accuracy.

V. SIMULATION RESULTS

In the simulation section, we reverse the order of discussion by first showing the accuracy of estimators in carrier synchronization and then showing some results of sequential detection since the GLRT based detector in (6) relies on the accuracy of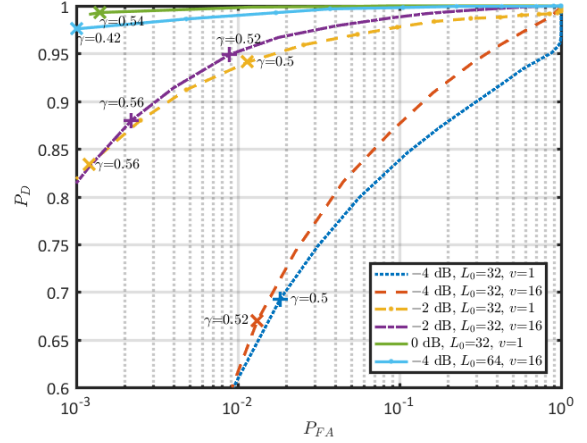 the SL estimator. The symbol sequence of the preamble is chosen as a Gold sequence with good autocorrelation property and modulated by a QPSK alphabet. The pulse is chosen a 0.5 rolloff Square-Root Raised Cosine (SRRC) pulse to satisfy the (squared root of) Nyquist property. The normalized frequency offset δ is intentionally set to be in the safe estimation range for all estimators for simulation purpose.

A. Simulation Results for Estimation

Figure 3 illustrates the accuracy of single-lag (SL) and the NM estimator. Compared with the two curves of SLs with $v=1$ and $v=16$, we see the length-16 partial correlating improves the accuracy of SL by providing an approximate 2.5 dB relative processing gain at negative SNRs (near SNR = −5 dB). Moreover, the SL with $v=1$ approaches the lower bound (19) with $v = 1$ at high SNRs while SL with $v=16$ does not. The gap is due to the Dirichlet function with respect to v and $|\delta|$ increases the variance. For the same reason, the accuracy of SL with $v=16$ at small frequency offset has a better accuracy at all SNRs.

The SL estimators don't approach the CRVB [9] while the NM does. We also see the NM estimator achieves a good accuracy based on the starting point of SL with $v = 16$ at lower SNR because the latter provides enough accuracy. In contrast, the NM estimator based on SL with $v = 1$ has worse accuracy than SL at all negative SNRs because the accuracy of SL is not enough so that the Newton iteration converges occasionally to other local minimum away from the true frequency offset.

Figure 4 compares the accuracy of our proposed estimators and traditional estimators in [3]–[5]. It shows when frequency offset is small, our NM estimator has a slightly better accuracy than traditional estimators at moderate SNRs. The drawback of NM estimator is the poor accuracy at low SNRs since it depends on the SL. Thus, a family of the SL with $v = 16$ and the NM based on the SL with $v = 1$ can be used to achieve a good accuracy at most SNRs.

B. Simulation Results for Detection

Figure 5 shows the receiver operating characteristics (ROC) of the detection algorithm. The better accuracy of SL with par-
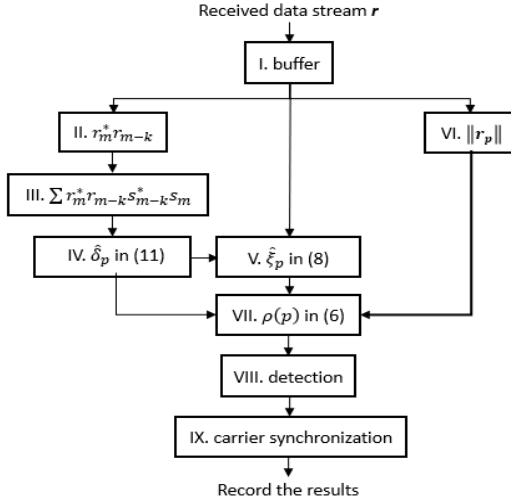
Fig. 6. Block diagram for implementing the proposed algorithm in TBB

4.5 GHz clock frequency. The results of Google benchmark for each node in Figure 6 are shown in Table II. Note, the time cost in the table refers to one buffer size of 8192 samples. The throughput of the pipeline is dominated by the node with the longest time. Thus, the ideal throughput is approximately equal to $8192/837253 \cdot 10^3 \approx 9.78$ MHz.

In operation, the throughput of the algorithm is in the range of 4.5 MS/s ~ 5.0 MS/s with latency near 1 ms; The detection algorithm is very robust and the false alarm probability is near 0 at moderate SNR.

REFERENCES

[1] D. D. Falconer, F. Adachi, and B. Gudmundson, "Time division multiple access methods for wireless personal communications," *IEEE Communications Magazine*, vol. 33, no. 1, pp. 50–57, 1995.

[2] M. Morelli and U. Mengali, "Feedforward frequency estimation for PSK: A tutorial review," *European Transactions on Telecommunications*, vol. 9, pp. 103–116, 1998.

[3] S. Kay, "A fast and accurate single frequency estimator," *IEEE Transactions on Acoustics, Speech, and Signal Processing*, vol. 37, no. 12, pp. 1987–1990, 1989.

[4] M. P. Fitz, "Further results in the fast estimation of a single frequency," *IEEE Transactions on Communications*, vol. 42, no. 234, pp. 862–864, 1994.

[5] M. Luise and R. Reggiannini, "Carrier frequency recovery in all-digital modems for burst-mode transmissions," *IEEE Transactions on Communications*, vol. 43, no. 2/3/4, pp. 1169–1178, 1995.

[6] B. Ramakrishnan, "Frame synchronization with large carrier frequency offsets: Point estimation versus hypothesis testing," in *2010 7th International Symposium on Communication Systems, Networks Digital Signal Processing (CSNDSP 2010)*, pp. 45–50, 2010.

[7] M. Chiani and M. Martini, "On sequential frame synchronization in awgn channels," *IEEE Transactions on Communications*, vol. 54, no. 2, pp. 339–348, 2006.

[8] Y. Liang, D. Rajan, and O. E. Eliezer, "Sequential frame synchronization based on hypothesis testing with unknown channel state information," *IEEE Transactions on Communications*, vol. 63, no. 8, pp. 2972–2984, 2015.

[9] F. Gini, R. Reggiannini, and U. Mengali, "The modified cramer-rao bound in vector parameter estimation," *IEEE Transactions on Communications*, vol. 46, no. 1, pp. 52–60, 1998.

[10] J. R. Michael Voss, Rafael Asenjo, *Pro TBB: C++ Parallel Programming with Threading Building Blocks*. 2019.

tial correlating at low SNRs also increases the performance of detection, e.g., at −2 dB SNR, $\gamma = 0.56$, the gap of false alarm probability P_{FA} is only 0.1% but the detection probability P_D of SL with $v=16$ is 5% larger than P_D of SL with $v=1$. The figure also shows the detector doesn't work well at −4 dB SNR if only 32 symbols of preamble are used; The performance is significantly improved by doubling the number of symbols.

VI. IMPLEMENTATION ON SOFTWARE-DEFINED RADIO

To demonstrate the practicality of our algorithms, we have implemented them in C++ on a general purpose processor (GPP). The different aspects of the algorithm are mapped to logical nodes in a pipelined, parallel processing atchitecture using Threading Building Blocks (TBB) [10].

Figure 6 shows a simple block diagram illustrating pipeline for the algorithm. Due to space constraints, we don't give the details of each node. It is necessary to discuss the node for computing the phasor estimate $\hat{\xi}$ (node V). The numerator of (8) performs a time-varying convolution, which cannot be computed efficiently via FFT. Our solution to increasing the computational efficiency is to use parallel programming of TBB. Specifically, (8) can be computed in three stages: 1. Compute several segments of $\sum r_n s_n^*$ in several nodes in parallel; 2. each node is then multiplied by $\hat{\delta}_{SL}$ at the middle index of the partial correlation. 3. Sum all the nodes together. Thus, (8) is computed more efficiently as

$$||s||^2 \cdot \hat{\xi} \approx \sum_{i=0}^{L-1} e^{-j\pi\delta \frac{N(2m+1)}{L}} \sum_{n=mN/L}^{(m+1)N/L-1} r_n s_n^*, \quad (21)$$

where L is the number of nodes. Thus, by using parallel programming, the efficiency of computing $\hat{\xi}$ is increased by L^2.

Now we show the results of the proposed algorithm in parallel programming on SDR. The signal are transmitted and received between two universal software radio peripheral (USRP) connected by a 5-Gigabit Ethernet cable to laptops. At the receiver side, the CPU includes 6 cores and 12 threads with